Fuel 316 (2022) 123412

Contents lists available at ScienceDirect

Fuel

journal homepage: www.elsevier.com/locate/fuel

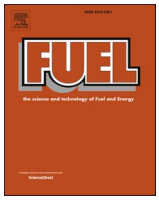

Full Length Article

A study on split diesel injection on thermal efficiency and emissions of an ammonia/diesel dual-fuel engine

Amin Yousefi *, Hongsheng Guo, Shouvik Dev, Simon Lafrance, Brian Liko

Energy, Mining and Environment Research Center, National Research Council Canada, 1200 Montreal Road, Ottawa, Ontario K1A 0R6, Canada

ARTICLE INFO

Keywords:
Split diesel injection
Ammonia/diesel dual-fuel combustion
Thermal efficiency
GHG emissions
Ammonia slip

ABSTRACT

Ammonia is gaining more interest as a carbon-free alternative fuel in freight transportation applications, especially the shipping industry. However, the problems of nitrous oxide (N_2O) emissions, which has almost 300 times higher global warming impact than carbon dioxide (CO_2), and ammonia slip have been the main challenges of using ammonia in compression ignition (CI) diesel engines. In this study, the effect of split diesel injection strategy (i.e., two-pulse diesel injection) on an ammonia/diesel dual-fuel (ADDF) engine is investigated under medium load operating conditions. Results indicate that the ADDF combustion mode with single diesel injection strategy achieves lower indicated thermal efficiency (ITE) compared to the corresponding diesel-only combustion mode. However, the use of split diesel injection strategy increases the ITE of the ADDF combustion mode to 39.72% which is higher than that obtained by diesel-only combustion mode (maximum ITE_{diesel} = 38.62%). Moreover, split diesel injection strategy reduces the unburned ammonia emissions of the ADDF combustion mode by up to 83.5% compared to the lowest unburned ammonia emissions achieved by single diesel injection strategy. Two split diesel injection strategies based on the optimum points of greenhouse gas (GHG) emissions are suggested in this research. At the first optimum point, the GHG emissions of the ADDF combustion mode are decreased by 23.7%, while ITE is increased by about 2% compared to the optimum point of diesel-only combustion mode. This, however, comes with about 10% higher nitrogen oxides (NO_x) emissions. The emitted GHG emissions of ADDF combustion can be further reduced by 30.6%, but at the expense of 2.2% lower ITE and 52.4% higher NO_x emissions than diesel-only combustion mode. At both optimum points, unburned ammonia emissions were significantly reduced to below 900 ppm compared to that of ADDF combustion mode with single diesel injection strategy (i.e., 4445 ppm). The lowest unburned ammonia concentration achieved in this study is still above the recommended exposure limit and therefore the use of appropriate after-treatment devices should be considered in the future.

1. Introduction

The impact of greenhouse gas (GHG) emissions on global warming has been a major driving force in internal combustion engine (ICE) technology development. The electrification of light-duty vehicles seems a near-term pathway to meet the requirements of substantially reduced emissions of carbon dioxide (CO_2) and other greenhouse gases. However, electrification of heavy-duty vehicles is currently not feasible due to the limited energy density and extended charging duration of batteries [1]. It is projected that compression ignition (CI) engines, which currently dominate the heavy-duty vehicle market, will continue to do so in the coming decades [2]. Utilizing alternative greener fuels and increasing fuel efficiency are promising approaches to curb the GHG emissions from heavy-duty transportation sector. As a carbon-free energy carrier, hydrogen (H_2) has the great potential for heavy-duty transportation, but issues related to its storage, distribution, and infrastructure deployment are delaying its full implementation [3]. Ammonia (NH_3), a hydrogen carrier, has recently attracted interest as a potential replacement of hydrocarbon fuels due to its carbon-free composition, relatively high energy density, and well-established and flexible infrastructure capable of mitigating hydrogen's key drawbacks [4–7]. Similar to hydrogen, the combustion of ammonia does not produce CO_2 emissions. Ammonia can also be synthesized from renewable energy sources (termed as "green ammonia"), thereby reducing its carbon footprint further [8–10]. Various enterprises are working towards commissioning of green ammonia manufacturing plants. For example, Yara, the world's second biggest ammonia producer, is scheduled to commence ammonia

* Corresponding author.
E-mail address: amin.yousefi@nrc-cnrc.gc.ca (A. Yousefi).

https://doi.org/10.1016/j.fuel.2022.123412
Received 8 December 2021; Received in revised form 15 January 2022; Accepted 21 January 2022
Available online 1 February 2022

Nomenclature

ADDF	Ammonia/Diesel Dual-Fuel
ASC	Ammonia Slip Catalyst
ASODI	After Start Of Diesel Injection
ATDC	After Top Dead Center
BMEP	Brake Mean Effective Pressure
CAD	Crank Angle Degree
CE	Combustion Efficiency
CFD	Computational Fluid Dynamic
CI	Compression Ignition
CO	Carbon Monoxide
CO_2	Carbon Dioxide
COV	Coefficient of Variation
DAQ	Data Acquisition
DI	Direct Injection
DOC	Diesel Oxidation Catalyst
DSR	Diesel Split Ratio
EODI	End Of Diesel Injection
EVC	Exhaust Valve Closing
EVO	Exhaust Valve Opening
FTIR	Fourier-Transform Infrared
GHG	Greenhouse Gas
HCCI	Homogeneous Charge Compression Ignition
HRR	Heat Release Rate
ICE	Internal Combustion Engine
IMEP	Indicated Mean Effective Pressure
IMO	International Maritime Organization
ISCO	Indicated Specific CO
$ISCO_2$	Indicated Specific CO_2
$ISCO_2$-equivalent	Indicated Specific CO_2-equivalent
ISHC	Indicated Specific HC
$ISNH_3$	Indicated Specific NH_3
ISN_2O	Indicated specific N_2O
$ISNO_x$	Indicated Specific NO_x
ITE	Indicated Thermal Efficiency
IVC	Intake Valve Closing
IVO	Intake Valve Opening
LHV	Lower Heating Value
KH-RT	Kelvin-Helmholtz Rayleigh-Taylor
NH_3	Ammonia
% NH_3	Ammonia Energy Fraction
NO_x	Nitrogen Oxides
N_2O	Nitrous Oxide
NYK	Nippon Yusen Kaisha
PPRR	Peak Pressure Rise Rate
RNG	Re-Normalization Group
RPM	Revolution Per Minute
SCR	Selective Catalytic Reduction
SOC	Start Of Combustion
SODI	Start Of Diesel Injection
TDC	Top Dead Center
UHC	Unburned Hydrocarbon
ULSD	Ultra-Low Sulfur Diesel

production from solar energy in Western Australia in 2023 [11]. Hy2Gen Inc. of Canada is planning to construct an ammonia production plant powered by hydro-electricity with a capacity of 500 tonnes of ammonia per day to be used as a fuel for the shipping industry [12]. Ammonia is being explored as a sustainable fuel solution for freight transportation, such as marine applications in particular.

Despite the merits associated with ammonia as a carbon-free fuel, there remain challenges for utilizing pure ammonia in CI engines, such as high auto-ignition temperature (924 K), low flame speed, and narrow flammability range [13,14]. Ammonia/diesel dual-fuel (ADDF) combustion is a feasible strategy to burn ammonia in CI engines [15,16]. In the ADDF combustion strategy, premixed ammonia-air mixture is introduced into the engine cylinder during the intake stroke, compressed during the compression stroke, and ignited by the direct injection (DI) of diesel at a desirable engine crank angle. Study of Bro et al. [17] in 1977 was the first investigation of utilizing ammonia in a diesel engine using ADDF combustion mode. They compared the performance of different premixed fuels such as ammonia, methanol, ethanol, and methane in a diesel engine. They found that the combustion of ammonia in a diesel engine has the longest ignition delay and lowest fuel efficiency than other tested fuels. In 2008 and 2011, Reiter et al. [18,19] observed that ADDF engine can obtain similar power output and lower CO_2 emissions than diesel engine. The nitrogen oxide (NO_x) emissions of ADDF mode can be lower than diesel mode if the energy fraction of ammonia is maintained below 40%. These came at the expense of ammonia slip (1000–3000 ppm) in ADDF combustion mode [18,19]. Recent concerns about global warming and increasingly severe emissions regulation are renewing the interest in the research and development of implementing ammonia in CI diesel engines. In 2018, Niki et al. [20] found that increasing energy fraction of ammonia from 0 to 30% deteriorates the fuel efficiency and increases the unburned ammonia and nitrous oxide (N_2O) emissions. In 2019, they tested diesel double injection to reduce the unburned ammonia emissions [16]. However, they found that N_2O emissions significantly increased when using double injection [16]. Bicer and Dincer [21] estimated that the life cycle GHG emissions (i.e., cradle to grave) of green ammonia-powered vehicles is about 56% lower than that of diesel-powered vehicles. Recently, MAN Energy Solutions [22] suggested ammonia as one of the most promising marine alternative fuels which can significantly reduce the GHG emissions within shipping industry. They aim to introduce the first ammonia/diesel dual-fuel marine engine into the market by 2024. Nippon Yusen Kaisha (NYK) shipping industry group aims to build ammonia-fueled ammonia-gas carrier vessels to cut GHG emissions from shipping by at least 50% by 2050 [23]. These actions are in line with International Maritime Organization (IMO)'s strategy to reduce GHG emissions of international shipping by at least 40% by 2030 and pursue efforts towards 70% reduction by 2050 compared to the 2008 level [24].

In a recent study [25], we investigated the effect of ammonia energy fraction and start of diesel injection (SODI) timing on combustion performance and emissions of an ADDF engine. It was found that increasing the energy fraction of ammonia increases the N_2O emissions. This offsets the benefit of lower CO_2 emissions of ADDF combustion mode and results in higher GHG emissions than diesel-only combustion mode at a constant SODI. However, advancing SODI decreases the GHG emissions of ADDF combustion mode by up to 12% compared to that of diesel-only combustion mode [25]. This comes at the expense of lower indicated thermal efficiency than diesel-only combustion mode and significant unburned ammonia emissions (i.e., 4000–5000 ppm) in the exhaust flow. In order to address these issues, this paper experimentally investigates the effect of split diesel injection (i.e., two-pulse diesel injection) on combustion performance and emissions of an ADDF engine under medium load conditions. Diesel injection parameters such as the start of diesel pre-injection (SODI-pre), start of diesel main-injection (SODI-main), and the ratio of the injected diesel in pre and main injections (%DSR) are carefully optimized to further decrease the unburned ammonia and GHG emissions of the ADDF combustion mode while achieving higher thermal efficiency than the diesel-only combustion mode. A computational fluid dynamic (CFD) model is also used to simulate the ADDF combustion at selected operating conditions to help understand the underlying mechanism of the experimental

observations.

2. Experimental apparatus and method

2.1. Engine test setup and emissions analyzer

The test setup is similar to that used in our previous studies [25–27]. A brief description is provided here for completeness. The engine employed was a modified Caterpillar 3401 heavy-duty, single-cylinder, four-stroke, CI diesel engine. The schematic of experimental setup is shown in Fig. 1 and the specifications of the stock engine are listed in Table 1. The original Caterpillar engine was modified to suit ammonia/diesel dual-fuel combustion by adding a gaseous fuel injector block in the intake manifold to introduce ammonia into the engine. An eddy current dynamometer was used to control the engine load during the experiments. In-cylinder pressure signal was collected by a Kistler Piezo-Star 6125C pressure transducer, which was flush-mounted on the cylinder head. The transducer output was converted into an analog signal using a Kistler charge amplifier and recorded using an AVL combustion analyzer. For each operating point, cylinder pressure data from 100 stable consecutive cycles was recorded at a resolution of 0.2 CAD. Engine operating conditions were monitored and recorded by a data acquisition (DAQ) system based on LabVIEW platform over three minutes for each steady-state operating point. The mean values of these operating parameters over the three minutes were used in post-processing. The steady-state condition was determined by the stabilization of the exhaust gas temperature for each measurement point. Exhaust gases were transferred to the emission analyzers using a heated sample line (T = 191 °C ± 1). The exhaust gas compositions (i.e., NH_3, CO, CO_2, HC, NO, NO_2, and N_2O) were monitored and recorded using an MKS Fourier-Transform Infra-Red (FTIR) series 2000 multi-gas analyzer over the three minute period for each steady-state test condition.

2.2. Air and fuel supply systems

The intake air feed system mainly consists of an external air compressor, a turbine type mass flow meter, a control valve, an air-heater/cooler, and an intake surge tank. The intake air was provided by an external compressor whose output pressure could be adjusted up to 5.50 bar. A Fisher-Emerson control valve was used to regulate the intake manifold air pressure according to the test requirements. A turbine type mass flow meter manufactured by Sierra Instruments Inc. was used to measure the intake air flow rate. The intake air temperature could be adjusted by a heating and cooling system to a range of temperatures from 10 to 80 °C. An intake surge tank was used before the intake manifold to reduce the pressure oscillations during the test.

Table 1
Engine specifications.

Engine model	Caterpillar 3401
Number of cylinders	1
Bore × Stroke (mm × mm)	137.2 × 165.1
Conn. rod length (mm)	261.62
Compression ratio	16.25
Displacement (L)	2.44
Intake valve opening (IVO)	−358.3 °ATDC
Intake valve closing (IVC)	−169.7 °ATDC
Exhaust valve opening (EVO)	145.3 °ATDC
Exhaust valve closing (EVC)	348.3 °ATDC

The diesel fuel was directly injected into the engine cylinder by a Ganser common-rail diesel injection system. The common-rail injection system was externally powered by a high-pressure fuel pump and was capable of producing diesel injection pressure up to 1800 bar. The diesel flow rate was measured by a Bronkhorst mini CORI-FLOW^{TM} mass flow meter. The ammonia supply system mainly consisted of ammonia cylinders with heated blankets, pressure regulators, a thermal mass flow meter, an ammonia gas chamber, and gas injectors installed in an injector block fitted into the intake manifold. The liquefied ammonia was stored in two 150 lb ammonia cylinders. A heated blanket system was used to keep the temperature of the cylinders at 38 °C and maintain the ammonia supply pressure. Ammonia flowed from the cylinders to a pressure regulator where the flow pressure was reduced and maintained at about 6.20 bar. The flow rate of ammonia was measured by a Bronkhorst thermal mass flow meter (EL-FLOW series). The final ammonia pressure before the injectors was regulated to approximately 4.82 bar by using a Bronkhorst pressure controller. The gaseous ammonia was fed into the intake manifold via two gas injectors (model Gs60, Alternative Fuel System Inc.) during the intake stroke. An ammonia gas chamber was placed before the gas injectors in the ammonia feed system to provide a stable ammonia mass flow during each injection. National Instruments hardware (PXI-1031 chassis with PXI-8184 embedded controller and 7813R RIO card connected to a cRIO-9151 expansion chassis) and LabVIEW-based software were used

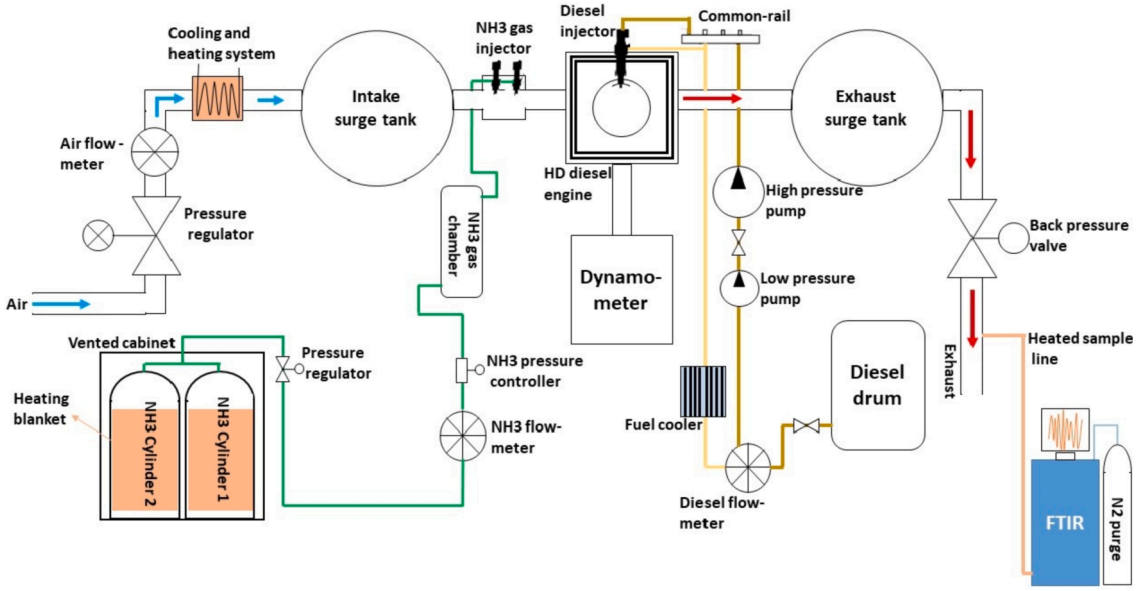

Fig. 1. Schematic diagram of engine test setup.

to control the injection timings, pulse widths, and injector pressures of both diesel and ammonia. Table 2 summarizes the main engine experimental instruments and their corresponding accuracies.

2.3. Properties of test fuels

The fuels employed in this experimental study are Canadian ultra-low sulfur diesel (ULSD) and anhydrous ammonia supplied by Linde, Canada. The main characteristics of both fuels are listed in Table 3.

2.4. Experimental methodology

Combustion analysis was performed based on the cylinder pressure and net heat release rate (HRR) traces. The net HRR was calculated using Eq. (1), where V is the cylinder volume, P is the cylinder pressure, and θ is the engine crank angle, and γ is the ratio of the specific heats.

$$HRR_{net} = \frac{\gamma}{\gamma - 1} P \frac{dV}{d\theta} + \frac{1}{\gamma - 1} V \frac{dP}{d\theta} \quad (1)$$

Based on the heat release rate, the combustion parameters such as CA10, CA50, and CA90 were determined as the engine crank angles at which 10%, 50%, and 90% of the cumulative heat were released, respectively. The CA10, CA50, and the interval from CA10 to CA90 were defined as the start of combustion (SOC), combustion phasing, and combustion duration, respectively. The pressure rise rate was calculated from the pressure profiles using Eq. (2).

$$\left(\frac{dP}{d\theta}\right)_n = \frac{P_{n+1} - P_n}{\Delta\theta} \quad (2)$$

The ammonia energy fraction (%NH_3), Eq. (3), was defined as the fraction of energy from ammonia in the total fuel energy input to the engine. Eqs. (4) and (5) show the indicated thermal efficiency (%ITE) and combustion efficiency (%CE). In these equations, $\dot{m}_D$ and $\dot{m}_{NH3}$ are the mass flow rate of diesel and ammonia, and LHV_{CO}, LHV_D, and LHV_{NH3} are the lower heating value of carbon monoxide, diesel, and ammonia, respectively. ISCO, ISHC, and $ISNH_3$ are the indicated specific emissions of CO, HC, and NH_3 respectively.

$$\%NH_3 = \frac{\dot{m}_{NH3} \times LHV_{NH3}}{\dot{m}_D \times LHV_D + \dot{m}_{NH3} \times LHV_{NH3}} \times 100 \quad (3)$$

$$\%ITE = \frac{Indicatedpower}{\dot{m}_D \times LHV_D + \dot{m}_{NH3} \times LHV_{NH3}} \times 100 \quad (4)$$

Table 2
Main experimental instruments and their accuracies.

Measured quantity	Instrument	Accuracy
Ammonia mass flow	Bronkhorst thermal mass flow meter (EL-FLOW series, model F-113AC)	±0.5% of measured value
Diesel mass flow	Bronkhorst flow mass flow meter (MINI-CORI)	±0.2% of measured value
Air mass flow	Sierra thermal mass flow meter (780S Flat Trak™)	±0.5% of measured value
Cylinder pressure	Kistler Piezo-Star 6125C pressure transducer	Cyclic temperature drift < ±0.3 bar
Crank angle	AVL 365C crank angle encoder	Mark resolution: 0.5 °CA, 0.1 °CA by means of multiplication
Emissions	MKS series 2000 multi-gas analyzer	±1% of calibrated range
Coolant, oil, ambient and charge air, and exhaust gas temperature	Thermocouple Type K	Temperature range of −40 to + 375 °C: ±1.5°C Temperature range of + 375 to + 1000 °C : ±0.4%
Ammonia and intake manifold air pressure	OMEGA pressure transducer (PX series)	±0.5% of compensated range

Table 3
Fuel properties.

Property	Ammonia	Diesel
Density (kg/m^3)	0.73 (@ 15 °C and 1.013 bar)	824.6 (@ 15 °C)
Cetane number	–	44.9
LHV (MJ/kg)	18.5	43.45
H/C ratio	–	1.78
Composition (%vol.)	NH3: 99.5–100%	–
Auto-ignition temperature (°C)	651 [11,28]	226–233 [29,30]
Maximum flame speed (m/s)	0.07 [11,28]	–
Stoichiometric air/fuel ratio	6.06 [11,28]	14.5 [29,30]
Latent heat of vaporization (kJ/kg)	1370 [11,28]	270 [29,30]
Flammability limit in air (%vol.)	15–28 [11,28]	0.6–6.5 [29,30]

$$\%CE = \left[1 - \frac{ISCO \times LHV_{CO} + ISHC \times LHV_D + ISNH_3 \times LHV_{NH3}}{\dot{m}_D \times LHV_D + \dot{m}_{NH3} \times LHV_{NH3}} \times indicatedpower\right] \times 100 \quad (5)$$

Diesel split ratio (%DSR) was defined as the ratio of pulse width of pre-injected diesel to the total diesel injection pulse width.

$$\%DSR = \frac{Pulsewidth_{pre-iniection}}{Pulsewidth_{total}} \times 100 \quad (6)$$

2.5. Experimental operating conditions

All tests were run at constant engine speed and brake mean effective pressure (BMEP) of 910 rpm and 8.10 bar, respectively. The selected engine load is equivalent to 50% of the full load. The ammonia energy fraction (i.e., %NH_3, calculated by Eq. (3)) was kept constant at 40% once the engine was switched to ADDF combustion mode. Further increase in the ammonia energy fraction was not conducted due to the limit in the current experimental setup for the supplied ammonia flow rate. The gaseous ammonia was injected at −355 °ATDC during the intake stroke into the intake air stream. The intake temperature, intake pressure, and exhaust back pressure were maintained at 40 °C, 1.35 bar, and 1.50 bar, respectively. Increasing the diesel injection pressure caused the peak pressure rise rate (PPRR) to exceed the engine hardware limit when sweeping the diesel injection timings. Therefore, the diesel injection pressure was set at 525 bar for both diesel-only and ADDF combustion modes. To prevent engine damage, the maximum PPRR was maintained below 15.0 bar/CAD. The coefficient of variation (COV) of indicated mean effective pressure (IMEP) was maintained below 5.0% in order to achieve stable combustion during the test.

Table 4 shows the experimental test matrix including combustion mode, diesel injection strategy, start and end of pre and main diesel injection (SODI-pre, SODI-main, EODI-pre, and EODI-main), diesel split ratio (%DSR, calculated by Eq. (6)), and flow rates of diesel and ammonia. The engine test was started at diesel-only combustion mode (Test 1). Only a single diesel injection strategy with the sweep of SODI was performed in this test to provide the baseline data for comparison purpose. The SODI retard and advance were limited by the CA50 of 12 °ATDC (late combustion) and the PPRR of 15.0 bar/CAD, respectively. The engine was then switched to ADDF combustion mode with single diesel injection strategy and a sweep of SODI was conducted (Test 2). Similar to the diesel-only combustion mode, the SODI retard and advance limits were based on the CA50 of 12.0 °ATDC and the PPRR of 15.0 bar/CAD, respectively. While the engine was operating in ADDF combustion mode, the diesel injection strategy was switched from single to split (or two-pulse) diesel injection in Test 3. Then the effect of the diesel split ratio (25 to 45% with 5% increment) on combustion

Table 4
Experimental test matrix.

Test No.	Combustion mode	Diesel injection strategy	SODI-pre (°ATDC)	EODI-pre (°ATDC)	SODI-main (°ATDC)	EODI-main (°ATDC)	DSR (%)	Diesel (kg/h)	NH_3 (kg/h)
1	Diesel	Single (sweep of SODI)	–	–	−14.2	2.28		3.38	0
					−16	−0.24		3.23	
					−18	−2.46	–	3.15	
					−20	−4.48		3.15	
					−24	−8.44		3.16	
					−27	−11.23		3.22	
2	ADDF	Single (sweep of SODI)	–	–	−14.2	−2.18		2.08	3.18
					−16	−4.25		2	3.06
					−18	−6.41	–	1.98	3.02
					−20	−8.38		1.97	3.04
					–22	−10.42		1.93	2.98
					−24	−12.31		1.96	3.01
3	ADDF	Double (sweep of %DSR)	−30	−26.28		−4.86	25	2.02	3.07
				−25.48		−5.45	30	1.98	3.07
				−24.78	−16	−6.30	35	1.99	3.05
				–23.95		−6.93	40	1.97	3.05
				–23.05		−7.50	45	2.01	3.03
4	ADDF	Double (sweep of SODI-pre)	−26	−19.99		−6.98		1.96	3.04
			−30	−24.00		−7.00		1.93	3.01
			−34	−27.96		−6.94		1.95	2.98
			−38	−31.09		−6.86		1.95	3.01
			−42	−35.91	−16	−6.86	40	1.90	2.97
			−46	−39.91		−686		1.87	2.91
			−50	−43.86		−6.79		1.85	2.87
			−54	−47.87		−6.80		1.88	2.88
			−57	−50.89		−6.84		1.85	2.90
			−61	−54.80		−6.69		1.90	2.87
5	ADDF	Double (sweep of SODI-main)	−57	−50.68	−14	−4.52		1.91	2.95
				−50.70	−16	−6.55	40	1.92	2.93
				−50.57	−18	−8.36		1.93	2.96
				−50.54	−20	−10.31		1.97	2.98

performance and emissions of ADDF engine was performed at fixed SODI-pre and SODI-main of −30 and −16 °ATDC, respectively. When %DSR was further increased to above 45%, the peak pressure rise rate exceeded the engine hardware limit, and when %DSR was decreased to below 25%, the delivery of the pre-injected diesel was not reliable due to the very short injection pulse width. Test 4 includes a sweep of SODI-pre while SODI-main and diesel split ratio were maintained at −16 °ATDC and 40% respectively. Finally, the effect of advancing SODI-main on the combustion performance and emissions of ADDF combustion mode was conducted in test 5. SODI-pre and %DSR were set to −57 °ATDC and 40%, respectively, in test 5.

Different combinations of SODI-pre, SODI-main, and %DSR were tested in this study. However, considering the engine operating limits and the optimum thermal efficiency and GHG emissions, the results of selected split diesel injection strategies are presented and discussed in this paper.

3. Numerical modeling

The numerical simulations were conducted using a commercial CFD software, CONVERGE v3.0 [31]. Since the details of adopted models and sub-models were outlined in authors' previous study [25], only a brief description is provided here. In order to implement the chemistry calculations, a transient chemical kinetics solver, termed as SAGE [31], was used in the CFD model. Ammonia and diesel chemical kinetics mechanism were adopted from Otomo et al. [32] (32 species and 213 reactions) and Frassoldati et al. [33] (98 species and 895 reactions), respectively. The two mechanism were merged and thoroughly tuned and validated against one dimensional laminar flame speed and ignition delay data. The merged mechanism consisted of 119 species and 1077 reactions. The details of merging and tuning the mechanism will be presented in a separate study in the future. Re-normalization Group (RNG) k-ε turbulence model was used to simulate the turbulent flow within the combustion chamber [34]. The Kelvin-Helmholtz Rayleigh-Taylor (KH-RT) instability mechanism was used to model the diesel droplet atomization and breakup [35].

An open cycle of the engine with full cylinder geometry and intake and exhaust manifolds was simulated in this study. Fig. 2 shows the engine geometry and cut-plane of the computational cells at a selected engine crank angle after start of combustion. The base grid sizes of 3.0 mm and 1.5 mm were used in the engine cylinder and intake and exhaust manifolds, respectively. A fixed embedding grid scaling method was added in certain regions such as diesel fuel injector and intake and exhaust valves to refine the grid to 0.375 mm. Adaptive mesh refinement was used to generate cell size of 0.1875 mm during the diesel spray and combustion process and efficiently resolve details in the regions of the turbulent flame front, diesel spray, and higher species concentration gradients [36].

The developed CFD model was already validated against the

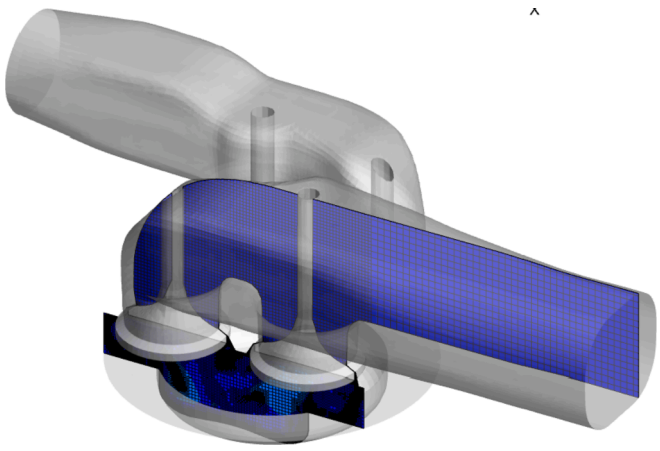

Fig. 2. Engine geometry and cut-plane of computational cells at a selected engine crank angle after start of combustion.

measured cylinder pressure, HRR, and emissions data of ADDF combustion under different ammonia energy fractions and a fixed SODI in authors' previous study [25]. The predicted cylinder pressure and HRR of ADDF combustion with single and split diesel injection strategies are also compared with their measured counterpart in Fig. 3. It is observed that the simulation results match the experimental data very well. The cylinder pressure before start of combustion, ignition timing, and cylinder peak pressure are excellently captured. The cylinder pressure and HRR during the expansion stroke are slightly over-predicted, which is probably due the assumption of constant boundary wall temperature in the simulations.

4. Results and discussion

4.1. Combustion characteristics

The experimental results of the effects of single and split diesel injection strategies on combustion characteristics of the investigated ADDF engine are presented and discussed in this section. These results include cylinder pressure and HRR curves, start of combustion, combustion phasing, combustion duration, and PPRR. The experimental results of the diesel-only combustion mode with single injection strategy are also added for comparison. CFD simulation of the local equivalence ratio, cylinder charge temperature, and OH radical distributions of some selected cases are also provided to shed more light on the underlying mechanisms of the ADDF combustion.

The effect of advancing SODI on cylinder pressure and HRR of ADDF combustion mode using single diesel injection strategy has been investigated in our previous study [25], but is shown again in Fig. 4a for comparison. It can be observed that advancing the SODI advances the SOC due to the earlier mixing between diesel and ammonia-air mixture. Advancing SODI also increases the cylinder peak pressure, because the earlier injection of diesel into the engine advances SOC and therefore more heat is released near the top dead center (TDC). Due to the same reason, the peak HRR increases when advancing SODI from −14.2 to –22 °ATDC. However, peak HRR starts to drop at SODI = −24 °ATDC probably due to the lower cylinder charge temperature when diesel is injected into the engine cylinder at such an early diesel injection timing.

Fig. 4b-d show the effects of %DSR, SODI-pre, and SODI-main on cylinder pressure and HRR of ADDF combustion mode with split diesel injection strategy. It can be observed from Fig. 4b that earlier injection of more diesel fuel (i.e., SODI-pre and SODI-main = −30 and −16 °ATDC) at any %DSR into the engine cylinder advances the SOC and increases the cylinder peak pressure compared to the single diesel

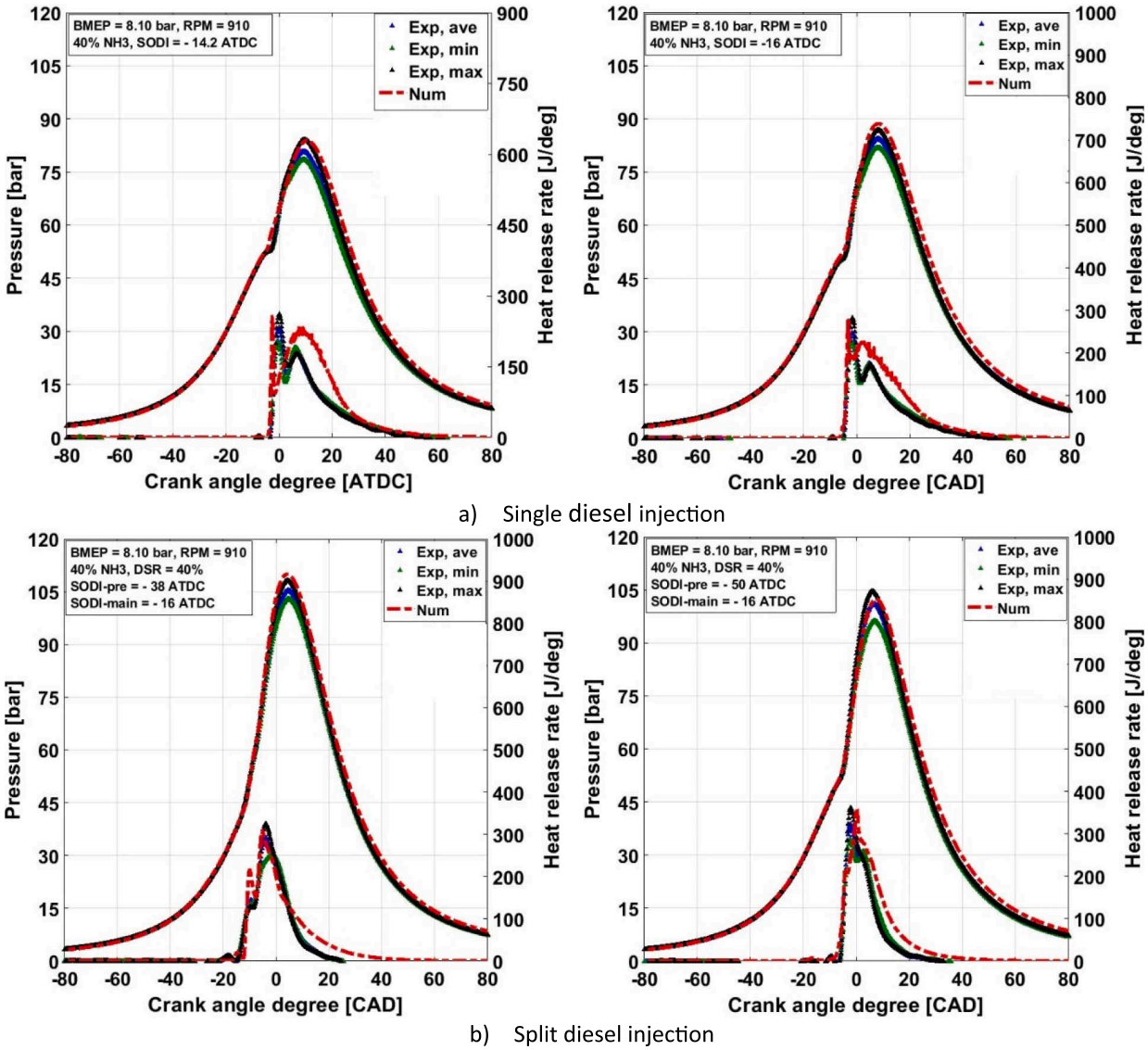

Fig. 3. Comparison of measured and calculated cylinder pressure and HRR of ADDF combustion mode with single and split diesel injection strategies.

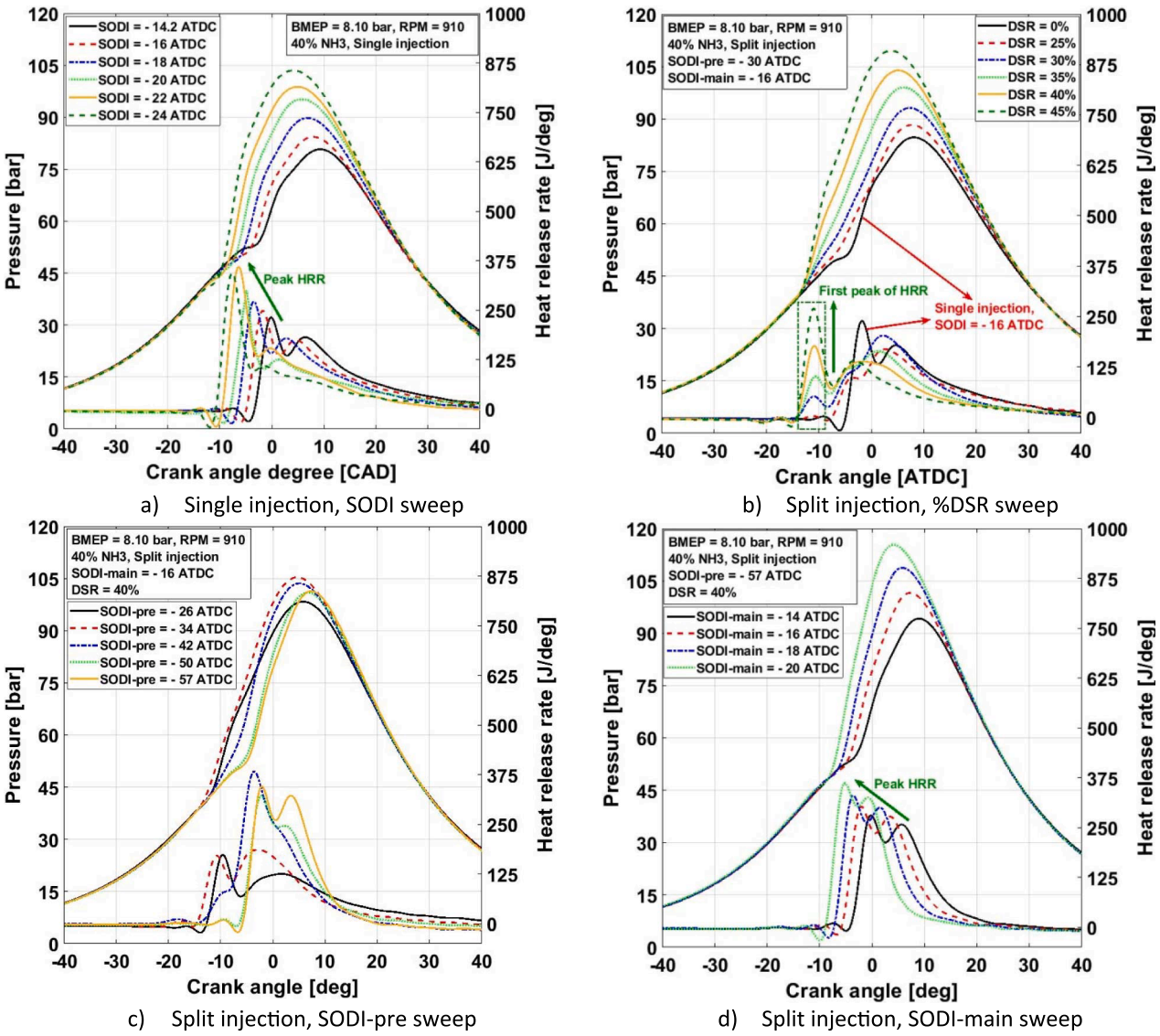

Fig. 4. Effect of single and split diesel injection strategies on cylinder pressure and HRR of ADDF combustion engine at BMEP = 8.10 bar and RPM = 910.

injection strategy at the SODI of −16 °ATDC. With increasing %DSR, this early injection of higher diesel quantity causes more diesel to be mixed with ammonia-air mixture sooner thereby increasing in-cylinder reactivity, which subsequently advances the SOC. Advanced SOC causes more heat to be released near TDC and therefore increases cylinder peak pressure. Increasing %DSR also increases the first peak of HRR, since more premixed mixture (i.e., pre-injected diesel and ammonia-air) is formed with increasing the %DSR and therefore more heat is released during the diesel-ammonia-air premixed combustion stage.

Fig. 4c shows that advancing SODI-pre to a certain crank angle (i.e., SODI-pre = −34 °ATDC) advances the SOC and increases the cylinder peak pressure. This is due to the earlier mixing between pre-injected diesel and ammonia-air mixture. However, further advancement of SODI-pre results in a longer ignition delay, retarded SOC, and decrease in cylinder peak pressure. Details on this will be discussed in Figs. 5 and 6 that follow.

As shown in Fig. 4d, advancing SODI-main advances the SOC and increases the cylinder peak pressure and HRR. This behavior is similar to advancing the SODI in a single diesel injection strategy shown in Fig. 4a.

Fig. 5a–c show the effects of single and split diesel injection strategies on CA10, CA50, and CA10-90 of ADDF combustion mode. The results of the diesel-only combustion mode with single diesel injection strategy are also added to these figures for comparison. As mentioned earlier, CA10, CA50, and CA10-90 represent the start of combustion, combustion phasing, and combustion duration, respectively. It can be observed that advancing SODI in the range of conventional diesel injection timings advances the SOC and combustion phasing and shortens the combustion duration of ADDF combustion mode with single diesel injection. These are primarily due to the earlier start of mixing between diesel and ammonia-air mixture and a larger number and wider spatial distribution of ignition kernels across the whole cylinder with advancing SODIs, which leads to earlier SOC and more heat release near TDC. A similar trend was observed in authors' previous studies when advancing start of diesel injection timing in a natural gas/diesel dual-fuel engine. More details can be found in [15,37].

Advancing the SODI-pre from −26 to −34 °ATDC advances the SOC and combustion phasing of ADDF combustion mode, but further advancement of SODI-pre retards the SOC and combustion phasing. To understand the mechanism behind this, the cylinder charge temperature and local equivalence ratio of ADDF combustion with retarded and advanced SODIs-pre of −30 °ATDC and −50 °ATDC, respectively, at 2 CAD after SODI-pre (°ASODI-pre) and at crank angle corresponding to SODI-main (i.e., CAD = −16 °ATDC) are presented and discussed in Fig. 6. In this figure, the contour plane is the YZ plane which passes

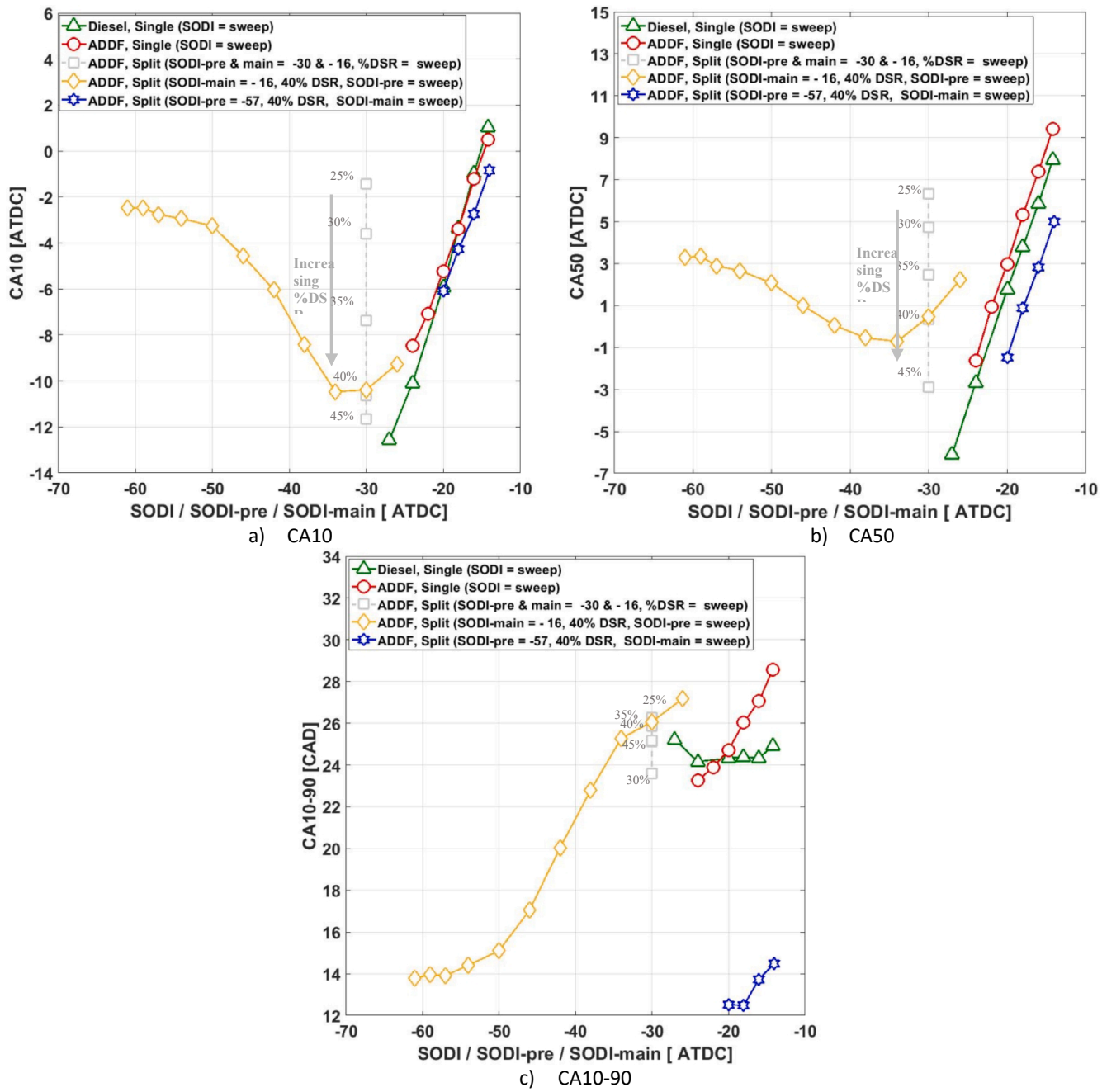

Fig. 5. Effect of single and split diesel injection strategies on CA10, CA50, and CA10-90 of ADDF combustion engine at BMEP = 8.10 bar and RPM = 910.

through the middle of two diesel plumes of the diesel spray. It is observed that at very advanced SODI-pre of −50 °ATDC, the cylinder charge temperature at 2 °ASODI-pre is relatively low ($T_{charge} \cong 600$ K). Therefore, the pre-injected diesel experiences relatively long evaporation process and mixes well with background ammonia-air during the ignition delay period. This can be found from the local equivalence ratio contour at CAD = −16 °ATDC where there is almost no locally rich air–fuel pockets (Fig. 6b). At this crank angle, the combustion temperature is high enough ($T_{charge} \cong 900$ K) but the premixed charge is very lean to be ignited early in the compression stroke, which causes that the SOC to be significantly delayed (i.e., SOC = −3.2 °ATDC) to after the diesel main-injection timing. However, at retarded SODI-pre of −30 °ATDC (Fig. 6a), the cylinder charge temperature at 2 °ASODI-pre is about $T_{charge} \cong 780$ K, which causes a shorter ignition delay and less mixing between diesel and ammonia-air mixture before SOC. The existence of locally rich air-fuel pockets and high cylinder charge temperature lead to an earlier SOC just a few crank angle after diesel main-injection timing (i.e., SOC = −10.4 °ATDC).

As shown in Fig. 5c, the combustion duration keeps reducing with the advancement of SODI-pre. At very advanced SODI-pre of −50 and −57 °ATDC, the HRR curve becomes similar to that encountered in a homogenous charge compression ignition (HCCI) mode (see Fig. 4c and d). To shed more light on this, the OH radical distributions (top-view) of ADDF combustion with retarded and advanced SODIs-pre of −30 °ATDC and −50 °ATDC, respectively, and fixed SODI-main of −16 °ATDC are compared and discussed in Fig. 7. In this figure the contour plane is parallel to the XY plane and is located at a vertical distance of 2 mm from the cylinder head to clearly show the ignition and flame kernels' growth in the central region of combustion chamber and piston squish area. It can be observed from Fig. 7a that for SODI-pre = −30 °ATDC the first

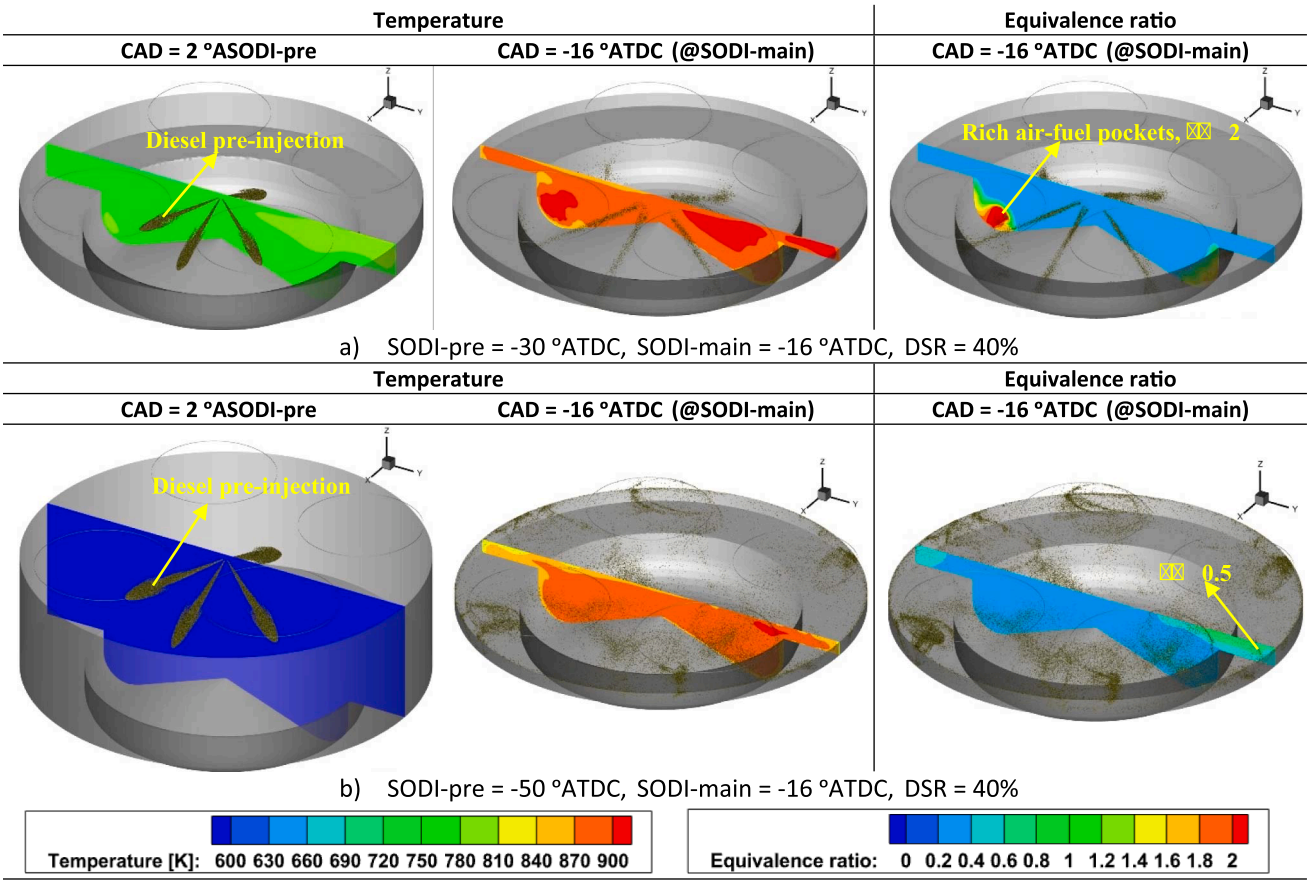

Fig. 6. Cylinder charge temperature and local equivalence ratio of ADDF combustion with split diesel injection strategy at two different SODIs-pre of a) −30 °ATDC and b) −50 °ATDC.

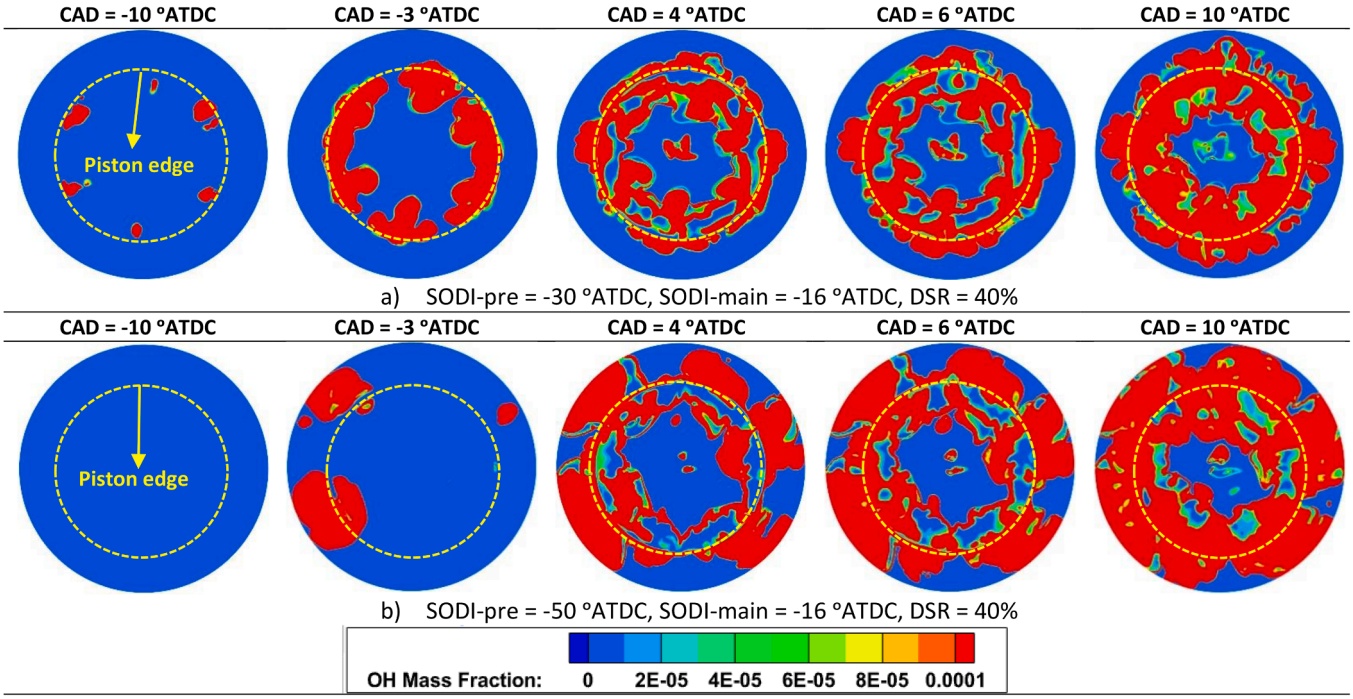

Fig. 7. OH distribution (top-view) of ADDF combustion with split diesel injection strategy at two different SODIs-pre of −30 °ATDC and −50 °ATDC.

ignition kernels (OH radicals) appear inside the piston bowl at an early engine crank angle of −10 °ATDC. The ignition kernels grow gradually inside the piston bowl and around the piston edge (CAD = −3 °ATDC). Flame propagation begins from these ignition kernels and they gradually spread towards the spray axes and center of combustion chamber (CADs = 4 and 6 °ATDC). The flame does not reach the very central regions of the engine cylinder and piston squish area until an engine crank angle of 10 °ATDC. This is mainly due to the poorer mixing between diesel and ammonia-air mixture in these regions. However, for SODI-pre = −50 °ATDC (Fig. 7b), the first ignition kernels do not appear in the piston squish area until a relatively late engine crank angle of −3 °ATDC, but the overall growth rate of the ignition kernels is faster (CAD = 4 °ATDC). The flame kernels propagate rapidly towards the center of combustion chamber and also piston squish area (CADs = 6 and 10 °ATDC) due to the better mixing between diesel and ammonia/air mixture. It can be summarized from the above discussion that at retarded SODIs-pre (e.g., SODI-pre = −30 °ATDC), the start of combustion is early. But due to the relatively poor mixing between diesel and ammonia-air mixture, combustion duration is relatively longer. For advanced SODI-pre (e.g., SODI-pre = −50 °ATDC), although the start of combustion is delayed, the flame propagates faster and combustion duration becomes shorter due to better mixing between diesel and ammonia-air mixture. This is similar to that in HCCI combustion mode.

Advancing SODI-main in ADDF combustion mode with split diesel injection strategy advances the SOC and combustion phasing and reduces the combustion duration (Fig. 5). This trend is similar to advancing the SODI in the single diesel injection strategy.

Fig. 8 shows the effects of single and split diesel injection strategies on the PPRR of ADDF combustion mode. It is observed that advancing the SODI of both diesel-only and ADDF combustion modes with single diesel injection strategy and even advancing SODI-main and/or increasing %DSR of ADDF combustion with split diesel injection strategy significantly increases the PPRR. These are mainly due to the advancement of combustion phasing and more intense heat release around the top dead center. However, for the split diesel injection strategy at the % DSR of 40%, the PPRR first decreases but then increases again with advancing SODI-pre. This is primarily related to the heat release at premixed combustion stage. With advancing SODI-pre from −28 to −34 °ATDC, the SOC advances and therefore premixed combustion happens at earlier crank angles relative to TDC (Fig. 4c and 5a), which causes lower PPRR. However, with further advancing of SODI-pre from −34 °ATDC, SOC retards and therefore premixed combustion happens at crank angles closer to TDC, which results in higher PPRR.

4.2. Indicated thermal efficiency, combustion efficiency, and emissions

The experimental results of the effects of single and split diesel injection strategies on indicated thermal efficiency, combustion efficiency, and emissions (CO_2, N_2O, GHG, NH_3, NO_x, unburned hydrocarbon (UHC) and carbon monoxide (CO)) of the investigated ADDF engine are presented in this section.

Fig. 9 shows the effects of single and split diesel injection strategies on the ITE and CE of ADDF combustion mode. It is observed that ADDF combustion mode with single diesel injection strategy achieves lower thermal efficiency compared to its counterpart diesel-only combustion mode at all examined SODIs. Advancing SODI from −14.2 to −20 °ATDC increases the ITE of both diesel and ADDF combustion modes with single diesel injection strategy, mainly due to the improved combustion efficiency (Fig. 9b) and more desirable combustion phasing (Fig. 5b). However, further advancement of SODI causes the ITE to drop. This is due to the overly advanced combustion phasing which causes a part of released energy from the fuel to work against the engine compression and therefore decrease the useful power and consequently the ITE.

The use of the split diesel injection strategy can significantly improve the ITE of ADDF combustion mode. It is observed that the ADDF combustion mode with split diesel injection strategy of SODI-pre = −46 °ATDC, SODI-main = −16 °ATDC and DSR = 40% obtains the highest ITE of 39.72% which is higher than those obtained by ADDF combustion mode with single injection strategy (maximum $ITE_{ADDF\text{-}single}$ = 38.36%) and even the highest ITE obtained by the counterpart diesel-only combustion mode (maximum $ITE_{diesel\text{-}single}$ = 38.62%). Overall, the use of advanced SODI-pre (e.g., SODIs-pre = −46 to −61 °ATDC) in ADDF combustion mode can provide enough premixing of pre-injected diesel and ammonia-air mixture which results in a high combustion efficiency as shown in Fig. 9b. This can be combined with appropriate SODI-main and %DSR to obtain a desirable combustion phasing and higher thermal

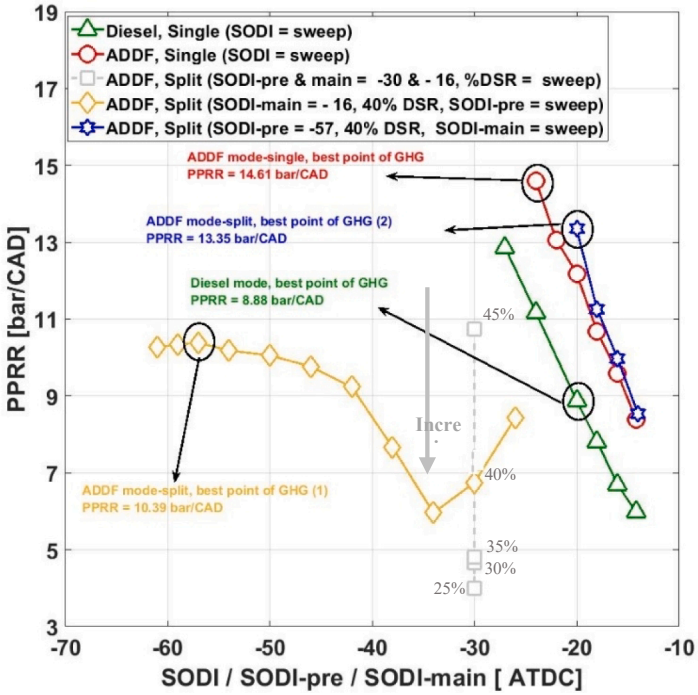

Fig. 8. Effect of single and split diesel injection strategies on PPRR of ADDF combustion engine at BMEP = 8.10 bar and RPM = 910.

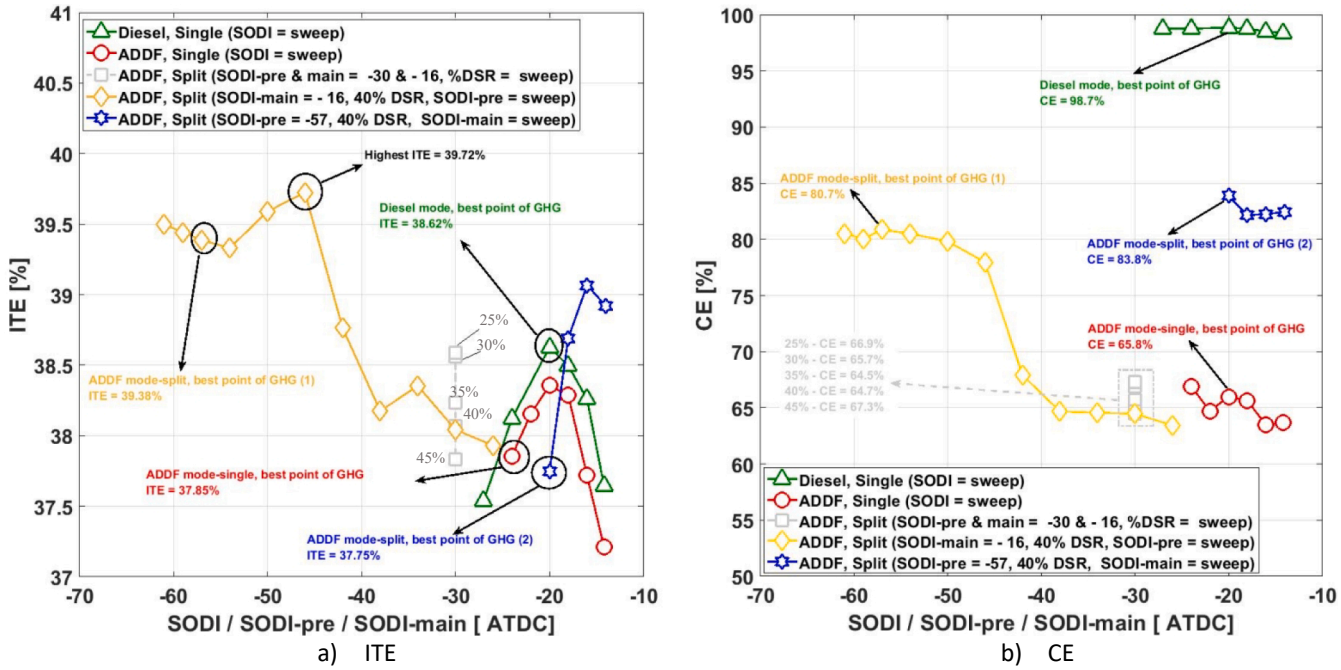

Fig. 9. Effect of single and split diesel injection strategies on indicated thermal efficiency and combustion efficiency of ADDF combustion engine at BMEP = 8.10 bar and RPM = 910.

efficiency compared to that of single diesel injection strategy.

Fig. 10a-c show the effect of single and split diesel injection strategies on indicated specific CO_2 ($ISCO_2$), N_2O (ISN_2O), and CO_2-equivalent ($ISCO_2$-equivalent) emissions of ADDF combustion mode. In this study, the CO_2-equivalent emission is calculated by Eq. (7).

$$ISCO_2 - \text{equivalent} = ISCO_2 + ISN_2O \times 300 \quad (7)$$

As shown in Fig. 10a, ADDF combustion mode produces lower CO_2 emissions than its counterpart diesel-only combustion mode. This is due to the fact that part of diesel fuel is replaced by ammonia whose combustion does not produce CO_2 emissions. It is also observed that using split diesel injection strategy can further decrease the CO_2 emissions of ADDF combustion mode compared to single diesel injection strategy due to the improvement of the ITE as shown in Fig. 9a.

It can be seen from Fig. 10b that diesel-only combustion mode produces negligible N_2O emission at all examined SODIs. However, the emissions of N_2O are one of the main concerns in ammonia combustion as the greenhouse gas impact of N_2O is about 300 times higher than that of CO_2 over a 100 year period [38]. Many studies have reported reactions $NH + NO \rightarrow N_2O + H$ and $NH_2 + NO_2 \rightarrow N_2O + H$ as the main pathways of N_2O formation, in which nitrogenous radicals (mainly NH and NH_2) react with NO and NO_2 at temperatures below 1400 K to form nitrous oxide [39–41]. It is seen from Fig. 10b that advancing the SODI of ADDF combustion mode with single diesel injection strategy decreases the ISN_2O emissions probably due to the increased combustion temperature. Moreover, using split diesel injection strategy with advanced SODI-pre (e.g., SODI-pre = −57 °ATDC) significantly decreases the ISN_2O emissions of ADDF combustion mode compared to that of single diesel injection strategy. Although advanced SODI-pre led to retarded start of combustion compared to single diesel injection strategy (Fig. 5a), it resulted in a very short combustion duration (Fig. 5c) which leads to more heat release near TDC and therefore increased combustion temperature. This can be also seen in Fig. 7b where the flame kernels almost reach the central region of combustion chamber and also piston squish area and that significantly increases the combustion temperature. This may help reduce ISN_2O emissions. The lowest ISN_2O emissions of 0.41 g/kW.h and 0.18 g/kW.h are achieved when sweeping SODI-pre and SODI-main, respectively. They are about 32.7% and 82.0% reductions compared to the lowest ISN_2O emissions of ADDF combustion mode with single diesel injection strategy (i.e., ISN_2O = 0.61 g/kW.h). This N_2O reduction significantly reduces $ISCO_2$-equivalent emissions of ADDF combustion mode with split diesel injection strategy compared to that with single diesel injection strategy, as shown in Fig. 10c. The lowest $ISCO_2$-equivalent emissions of ADDF combustion mode with single diesel injection strategy is 606.20 g/kW.h which occurs at the most advanced examined SODI of −24 °ATDC. The $ISCO_2$-equivalent emissions of ADDF combustion mode are further decreased to 525.51 g/kW.h (optimum GHG 1) and 478.10 g/kW.h (optimum GHG 2) when using split diesel injection strategies of SODI-pre = −57 °ATDC, SODI-main = −16 °ATDC, and %DSR = 40 and SODI-pre = −57 °ATDC, SODI-main = −20 °ATDC, and %DSR = 40, respectively. They are about 23.7% and 30.6% reductions compared to the optimum point of diesel-only combustion mode (i.e., optimum $GHG_{diesel-only}$ = 688.58 g/kW.h).

Fig. 11a–d show the effect of single and split diesel injection strategies on indicated specific NH_3 ($ISNH_3$), NO_x ($ISNO_x$), HC (ISHC), and CO (ISCO) emissions of ADDF combustion mode. Note that NO_2 emissions were negligible and outside the detection limit of the FTIR emission analyzer (i.e., below 10 ppm in most of the tests), and therefore NO is the only component of NO_x in this study. As shown in Fig. 11a, significant unburned ammonia emissions are detected when using single diesel injection strategy in ADDF combustion mode. The lowest indicated unburned ammonia emission is 15.53 g/kW.h (concentration of about 4445 ppm) which occurs at the most advanced SODI of −24 °ATDC. Split diesel injection strategy with advanced SODI-pre can significantly reduce the unburned ammonia emissions of ADDF combustion. At advanced SODIs-pre (e.g., SODI-pre = −50 °ATDC), the flame kernels almost reach the central region of combustion chamber and also piston squish area (see Fig. 7b) and that significantly reduces the unburned ammonia emissions. It is seen that the lowest unburned ammonia emissions of 3.20 g/kW.h (concentration of 893 ppm) and 2.56 g/kW.h (concentration of 721 ppm) are obtained when sweeping SODI-pre and SODI-main, respectively, in ADDF combustion mode with split diesel injection strategy. They are about 79.3% and 83.5% reduction compared to the lowest unburned ammonia emissions in ADDF mode with single diesel injection strategy. However, these levels of ammonia emissions

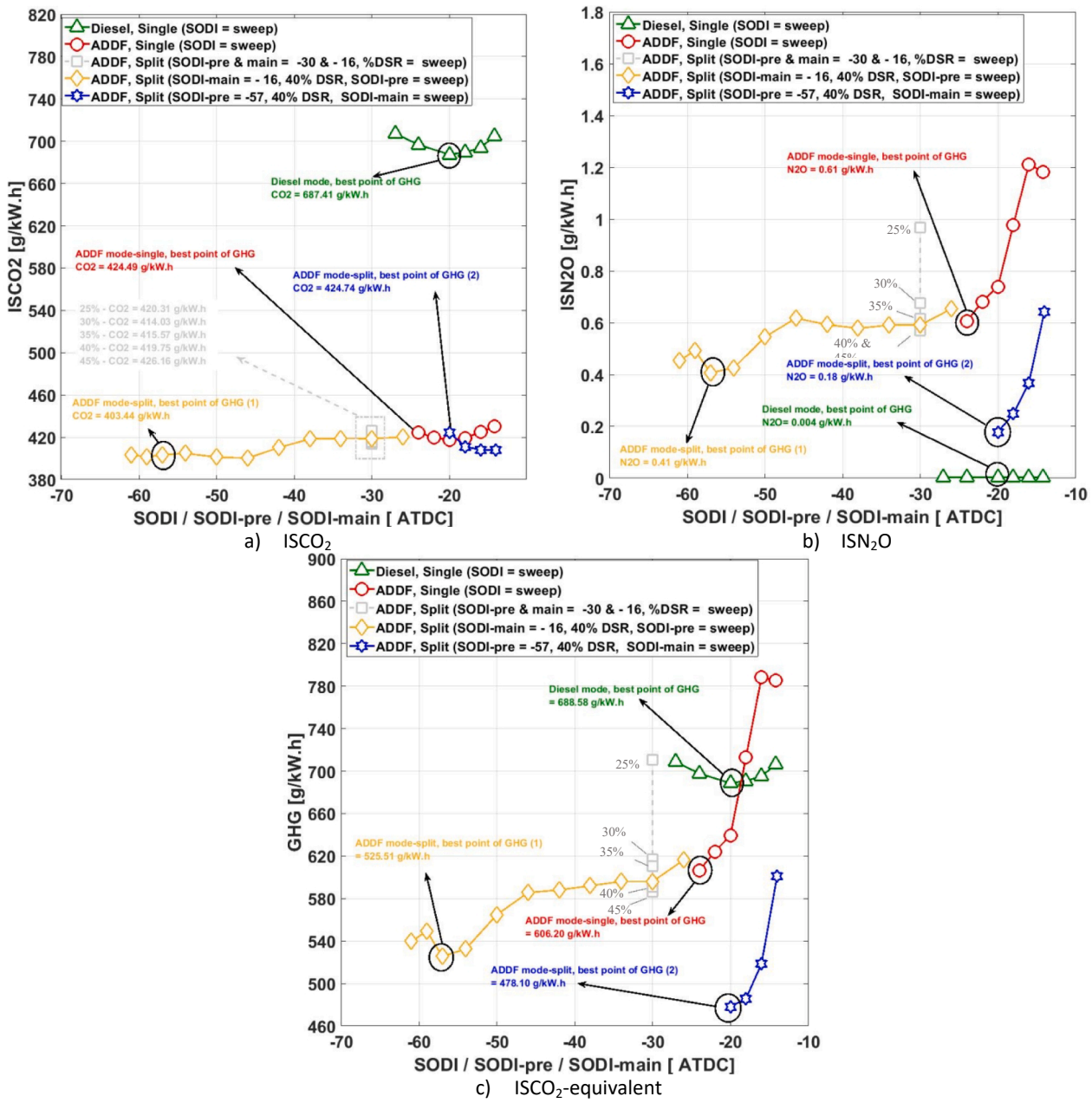

Fig. 10. Effect of single and split diesel injection strategies on $ISCO_2$, ISN_2O, and $ISCO_2$-equivalent emissions of ADDF combustion engine at BMEP = 8.10 bar and RPM = 910.

are still hazardous for human health [42]. Therefore, further study is required to investigate a combination of combustion strategies and appropriate exhaust after-treatment devices to further reduce ammonia emissions in the exhaust in the future.

Advancing SODI significantly increases the $ISNO_x$ emissions for both diesel-only and ADDF combustion modes with single diesel injection strategy (Fig. 11b). At a fixed SODI, however, the NO_x emissions of ADDF combustion mode with the single diesel injection strategy are lower than its counterpart diesel-only combustion mode. This is mainly due to the occurrence of the thermal $deNO_x$ process in ADDF combustion mode where excess NH_3 inside the combustion chamber plays the role of a thermal $deNO_x$ agent and reduces NO_x emissions. More details of the $deNO_x$ process in ADDF combustion mode can be found in the authors' previous study [25]. It can be seen that the $ISNO_x$ emissions of ADDF combustion with split diesel injection strategy depend on %DSR, SODI-pre, and SODI-main. The $ISNO_x$ emissions increase sharply by increasing %DSR and/or advancing SODI-main. This is mainly due to the combination of very advanced SOC (Fig. 5a) and short combustion duration (Fig. 5c) which leads to a significant increase of the combustion temperature and consequently a sharp increase in NO_x emissions. However, the $ISNO_x$ emissions gradually increase with the advancement of SODI-pre. Combustion duration shortens with the advancement of SODI-pre and this increases the combustion temperature. However, the start of combustion retards which tends to decrease the combustion temperature. As a combination of these two competing factors, the increase of combustion temperature is more gradual which leads to a gradual increase in NO_x emissions as advancing SODI-pre.

Fig. 11c and d show that the HC and CO emissions of ADDF combustion mode with single diesel injection strategy are higher than its counterpart diesel-only combustion mode. This is probably due to the lower combustion temperature of ADDF combustion mode compared to diesel-only mode. Split diesel injection strategy further increases the CO

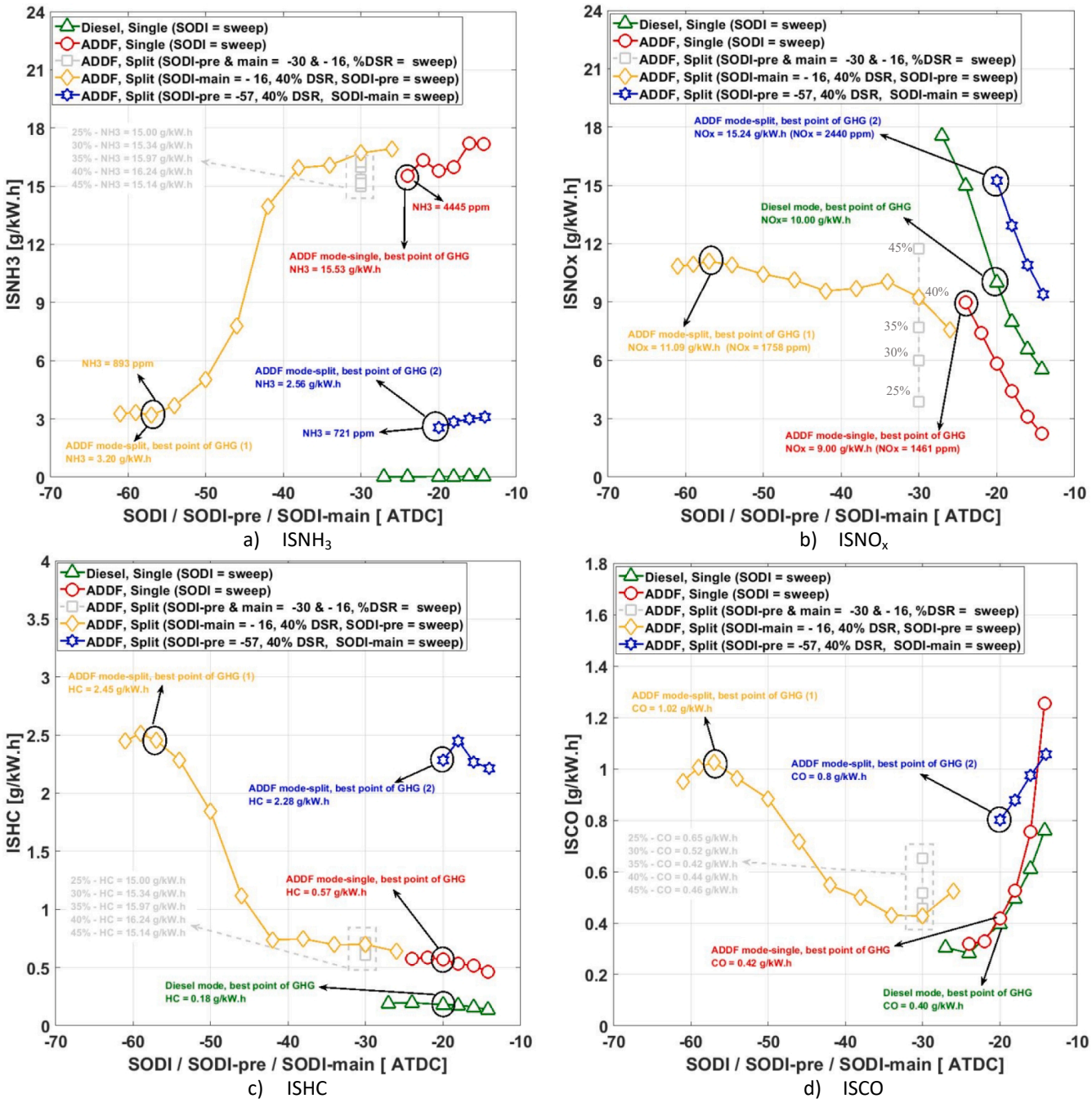

Fig. 11. Effect of single and split diesel injection strategies on $ISNH_3$, $ISNO_x$, ISCO, and ISHC emissions of ADDF combustion engine at BMEP = 8.10 bar and RPM = 910.

and HC emissions of ADDF combustion mode, especially when using advanced SODI-pre (e.g., SODI-pre = −57 °ATDC). This is probably due to the impingement of a part of diesel fuel on the cylinder wall, which leads to incomplete combustion and a significant increase in HC and CO emissions. Note that the use of after-treatment devices such as a diesel oxidation catalyst (DOC) may help to overcome the drawbacks of the high HC and CO emissions since the exhaust gas temperatures are higher than the DOC light-off temperature (i.e., $T_{exh} \cong 410–470$ °C).

It is interesting to compare the thermal efficiency and emissions (i.e., NO_x, NH_3, CO, and HC) of ADDF combustion with those of diesel-only combustion mode at the optimum point of GHG emissions. In this study, two optimum points of GHG emissions were identified when using split diesel injection strategy in ADDF combustion mode as shown in Fig. 10c. At the first optimum point, called GHG (1), corresponding to split diesel injection strategy of SODI-pre = −57 °ATDC, SODI-main = −16 °ATDC, and %DSR = 40%, the $ISCO_2$-equivelent emissions of ADDF combustion mode were decreased by 23.7% and ITE was increased by about 2% compared to the best of diesel-only combustion mode. This, however, came at the expense of 10% higher NO_x emissions compared to the optimum GHG point of diesel-only combustion mode. At the second optimum point, called GHG (2), corresponding to the split diesel injection strategy of SODI-pre = −57 °ATDC, SODI-main = −20 °ATDC, and %DSR = 40%, the $ISCO_2$-equivelent emissions of ADDF combustion further decreased by 30.6% compared to the best of diesel-only combustion, but ITE was decreased by 2.2% and NO_x emissions were increased by 52.4%. In both optimum points, unburned ammonia emissions also dropped below 900 ppm compared to that of ADDF combustion mode with single diesel injection strategy (i.e., 4445 ppm).

5. Conclusions

This study has experimentally investigated the effect of split diesel injection strategy on an ammonia/diesel dual-fuel engine with the objectives of improving the thermal efficiency and reducing GHG and unburned ammonia emissions. Tests were conducted at a medium engine load of BMEP of 8.10 bar and an engine speed of 910 rpm. The main findings of this research are summarized as follows.

- ADDF combustion mode with single diesel injection strategy achieved lower ITE compared to its counterpart diesel-only combustion mode at all examined SODIs. However, the use of split diesel injection strategy increased the ITE of ADDF combustion mode up to 39.72%. This is higher than those obtained by ADDF combustion mode with single injection strategy (the maximum $ITE_{ADDF\text{-}single}$ of 38.36%) and diesel-only combustion mode (the maximum $ITE_{diesel\text{-}single}$ of 38.62%).
- The lowest GHG emissions of ADDF combustion mode with single diesel injection strategy was 606.20 g/kW.h. This was further reduced to 478.10 g/kW.h by implementing split diesel injection strategies. This is about 30.6% GHG emissions reduction compared to the lowest GHG emissions of diesel-only combustion mode (i.e., 688.58 g/kW.h). Moreover, split diesel injection strategy reduced unburned ammonia emissions of ADDF combustion mode by up to 83.5% compared to the lowest level achieved by single diesel injection strategy.
- Two optimum points of GHG emissions were suggested in this research. At the first optimum point, the GHG emissions of ADDF combustion mode were decreased by 23.7% and ITE was also increased by about 2% compared to the best of diesel-only combustion mode. This, however, came with 10% higher NO_x emissions compared to the optimum GHG point of diesel-only combustion mode. GHG emissions of ADDF combustion can be further reduced by 30.6%, but at the expense of 2.2% lower ITE and 52.4% higher NO_x emissions than diesel-only combustion mode. At both optimum points, unburned ammonia emissions were significantly reduced to below 900 ppm compared to that of ADDF combustion mode with single diesel injection strategy (i.e., 4445 ppm). The lowest unburned ammonia concentration achieved in this study was still above the recommended exposure limit and therefore the use of appropriate exhaust gas after-treatment devices must be considered in the future.

Declaration of Competing Interest

The authors declare that they have no known competing financial interests or personal relationships that could have appeared to influence the work reported in this paper.

Acknowledgment

Funding of the experimental and numerical works was provided by National Research Council Canada (NRC) through the internal Advanced Clean Energy (ACE) Program. The numerical simulation was supported by CONVERGENT Science Inc.

References

[1] Senecal PK, Leach F. Diversity in transportation: Why a mix of propulsion technologies is the way forward for the future fleet. Results Eng 2019;4:100060. https://doi.org/10.1016/j.rineng.2019.100060.
[2] Annual Energy Outlook 2019 with projections to 2050. US Energy Inf Agency 2019.
[3] Chai WS, Bao Y, Jin P, Tang G, Zhou L. A review on ammonia, ammonia-hydrogen and ammonia-methane fuels. Renew Sustain Energy Rev 2021;147:111254. https://doi.org/10.1016/j.rser.2021.111254.
[4] Filipe Ramos C, Rocha RC, Oliveira PMR, Costa M, Bai X-S. Experimental and kinetic modelling investigation on NO, CO and NH3 emissions from NH3/CH4/air premixed flames. Fuel 2019;254:115693. https://doi.org/10.1016/j.fuel.2019.115693.
[5] Ichimura R, Hadi K, Hashimoto N, Hayakawa A, Kobayashi H, Fujita O. Extinction limits of an ammonia/air flame propagating in a turbulent field. Fuel 2019;246:178–86. https://doi.org/10.1016/j.fuel.2019.02.110.
[6] Wang S, Wang Z, Elbaz AM, Han X, He Y, Costa M, et al. Experimental study and kinetic analysis of the laminar burning velocity of NH3/syngas/air, NH3/CO/air and NH3/H2/air premixed flames at elevated pressures. Combust Flame 2020;221:270–87. https://doi.org/10.1016/j.combustflame.2020.08.004.
[7] Han X, Wang Z, He Y, Liu Y, Zhu Y, Konnov AA. The temperature dependence of the laminar burning velocity and superadiabatic flame temperature phenomenon for NH3/air flames. Combust Flame 2020;217:314–20. https://doi.org/10.1016/j.combustflame.2020.04.013.
[8] Feng Y, Zhu J, Mao Y, Raza M, Qian Y, Yu L, et al. Low-temperature auto-ignition characteristics of NH3/diesel binary fuel: Ignition delay time measurement and kinetic analysis. Fuel 2020;281:118761. https://doi.org/10.1016/j.fuel.2020.118761.
[9] Goldmann A, Dinkelacker F. Approximation of laminar flame characteristics on premixed ammonia/hydrogen/nitrogen/air mixtures at elevated temperatures and pressures. Fuel 2018;224:366–78. https://doi.org/10.1016/j.fuel.2018.03.030.
[10] Hayakawa A, Goto T, Mimoto R, Arakawa Y, Kudo T, Kobayashi H. Laminar burning velocity and Markstein length of ammonia/air premixed flames at various pressures. Fuel 2015;159:98–106. https://doi.org/10.1016/j.fuel.2015.06.070.
[11] Valera-Medina A, Xiao H, Owen-Jones M, David WIF, Bowen PJ. Ammonia for power. Prog Energy Combust Sci 2018;69:63–102. https://doi.org/10.1016/j.pecs.2018.07.001.
[12] Hy2gen canada inc. Https://Hy2genCom/Canada/n.d.
[13] Xiao H, Lai S, Valera-Medina A, Li J, Liu J, Fu H. Study on counterflow premixed flames using high concentration ammonia mixed with methane. Fuel 2020;275:117902. https://doi.org/10.1016/j.fuel.2020.117902.
[14] Xia Yu, Hashimoto G, Hadi K, Hashimoto N, Hayakawa A, Kobayashi H, et al. Turbulent burning velocity of ammonia/oxygen/nitrogen premixed flame in O2-enriched air condition. Fuel 2020;268:117383. https://doi.org/10.1016/j.fuel.2020.117383.
[15] Yousefi A, Guo H, Birouk M. Effect of diesel injection timing on the combustion of natural gas/diesel dual-fuel engine at low-high load and low-high speed conditions. Fuel 2019;235:838–46. https://doi.org/10.1016/j.fuel.2018.08.064.
[16] Niki Y, Nitta Y, Sekiguchi H, Hirata K. Diesel fuel multiple injection effects on emission characteristics of diesel engine mixed ammonia gas into intake air. J Eng Gas Turbines Power 2019;141. https://doi.org/10.1115/1.4042507.
[17] Bro K, Pedersen PS. Alternative diesel engine fuels: An experimental investigation of methanol, ethanol, methane and ammonia in a D.I. diesel engine with pilot injection. SAE Tech Pap 1977. https://doi.org/10.4271/770794.
[18] Reiter AJ, Kong S-C. Demonstration of compression-ignition engine combustion using ammonia in reducing greenhouse gas emissions. Energy Fuels 2008;22(5):2963–71. https://doi.org/10.1021/ef800140f.
[19] Reiter AJ, Kong S-C. Combustion and emissions characteristics of compression-ignition engine using dual ammonia-diesel fuel. Fuel 2011;90(1):87–97. https://doi.org/10.1016/j.fuel.2010.07.055.
[20] Niki Y, Nitta Y, Sekiguchi H, Hirata K. Emission and combustion characteristics of diesel engine fumigated with ammonia. ASME 2018 Intern Combust Engine Div Fall Tech Conf ICEF 2018 2018;1:1–7. https://doi.org/10.1115/ICEF2018-9634.
[21] Bicer Y, Dincer I. Life cycle assessment of ammonia utilization in city transportation and power generation. J Clean Prod 2018;170:1594–601. https://doi.org/10.1016/j.jclepro.2017.09.243.
[22] MAN B&W two-stroke engine operating on ammonia. Man Energy Solut n.d.
[23] NYK Green Business. NYK ' s view on the use of Ammonia as Marine Fuel NYK Group Fleet and Facility Ammonia as a green shipping fuel: challenges and opportunities Digital Workshop 23rd September 2021 2021.
[24] International Maritime Organization (IMO). IMO Action To Reduce GHG Emissions From International Shipping 2019.
[25] Yousefi A, Guo H, Dev S, Liko B, Lafrance S. Effects of ammonia energy fraction and diesel injection timing on combustion and emissions of an ammonia/diesel dual-fuel engine. Fuel 2021:122723. https://doi.org/10.1016/j.fuel.2021.122723.
[26] Yousefi A, Guo H, Dev S, Liko B, Lafrance S. Effect of pre-main-post diesel injection strategy on greenhouse gas and nitrogen oxide emissions of natural gas/diesel dual-fuel engine at high load conditions. Fuel 2021;302:121110. https://doi.org/10.1016/j.fuel.2020.120071.
[27] Yousefi A, Guo H, Birouk M, Liko B, Lafrance S. Effect of post-injection strategy on greenhouse gas emissions of natural gas/diesel dual-fuel engine at high load conditions. Fuel 2021;290:120071. https://doi.org/10.1016/j.fuel.2020.120071.
[28] Kobayashi H, Hayakawa A, Somarathne KDK, Okafor E. Science and technology of ammonia combustion. Proc Combust Inst 2019;37(1):109–33. https://doi.org/10.1016/j.proci.2018.09.029.
[29] Zabetakis MG. Flammability characteristics of combustible gases and vapors. US Dep Inter Bur Mines Bull 1965;627:20–7.
[30] Setchkin NP. Self-ignition temperatures of combustible liquids. J Res Natl Bur Stand 1934;1954(53):49. https://doi.org/10.6028/jres.053.007.
[31] Richards K.J. SPK and PE. Converge Manual. Converg (Version 24) Manual," Converg Sci Inc, Madison, Wisconsin, USA 2017.
[32] Otomo J, Koshi M, Mitsumori T, Iwasaki H, Yamada K. Chemical kinetic modeling of ammonia oxidation with improved reaction mechanism for ammonia/air and ammonia/hydrogen/air combustion. Int J Hydrogen Energy 2018;43(5):3004–14. https://doi.org/10.1016/j.ijhydene.2017.12.066.
[33] Frassoldati A, D'Errico G, Lucchini T, Stagni A, Cuoci A, Faravelli T, et al. Reduced kinetic mechanisms of diesel fuel surrogate for engine CFD simulations. Combust

Flame 2015;162(10):3991–4007. https://doi.org/10.1016/j.combustflame.2015.07.039.
[34] Yakhot V, Orszag SA, Thangam S, Gatski TB, Speziale CG. Development of turbulence models for shear flows by a double expansion technique. Phys Fluids A 1992;4(7):1510–20. https://doi.org/10.1063/1.858424.
[35] Reitz RD, Beale JC. Modeling spray atomization with the Kelvin-Helmholtz/Rayleigh-Taylor hybrid model. At Sprays 1999;9(6):623–50.
[36] Senecal PK, Richards KJ, Pomraning E, Yang T, Dai MZ, McDavid RM, et al. A New Parallel Cut-Cell Cartesian CFD Code for Rapid Grid Generation Applied to In-Cylinder Diesel Engine Simulations 2007;2007:776–90. https://doi.org/10.4271/2007-01-0159.
[37] Yousefi A, Guo H, Birouk M. An experimental and numerical study on diesel injection split of a natural gas/diesel dual-fuel engine at a low engine load. Fuel 2018;212:332–46. https://doi.org/10.1016/j.fuel.2017.10.053.
[38] Https://WwwEpaGov/Ghgemissions/Understanding-Global-Warming-Potentials Accessed 2017:1–5.
[39] Mathieu O, Petersen EL. Experimental and modeling study on the high-temperature oxidation of Ammonia and related NOx chemistry. Combust Flame 2015;162(3):554–70. https://doi.org/10.1016/j.combustflame.2014.08.022.
[40] Duynslaegher C, Jeanmart H, Vandooren J. Flame structure studies of premixed ammonia/hydrogen/oxygen/argon flames: Experimental and numerical investigation. Proc Combust Inst 2009;32 2009;32(1):1277–84. https://doi.org/10.1016/j.proci.2008.06.036.
[41] Nakamura H, Hasegawa S, Tezuka T. Kinetic modeling of ammonia/air weak flames in a micro flow reactor with a controlled temperature profile. Combust Flame 2017;185:16–27. https://doi.org/10.1016/j.combustflame.2017.06.021.
[42] Ammonia as a refrigerant of choice. ASHRAE 2017:43.